Grazing-incidence X-ray fluorescence analysis of thin chalcogenide materials deposited on Bragg mirrors

E. Nolot, W. Pessoa, S. Torrengo, Y. Mazel, M. Bernard, P. Gergaud, Yves Ménesguen, Marie-Christine Lépy, D. Eichert

Version of Record: https://www.sciencedirect.com/science/article/pii/S0584854719305944
Manuscript_638a30d59a6af8f89d82ae91e07ddf3b

Grazing-Incidence X-ray Fluorescence analysis of thin chalcogenide materials deposited on Bragg mirrors

E. Nolot[1*], W. Pessoa[1], S. Torrengo[1], Y. Mazel[1], M. Bernard[1], P. Gergaud[1], Y. Ménesguen[2], M.C Lépy[2], D. Eichert[3]

[1] *Univ. Grenoble Alpes, CEA, LETI, F-38000 Grenoble*
[2] *CEA, LIST, Laboratoire National Henri Becquerel (LNE-LNHB), F-91191 Gif-sur-Yvette Cedex, France*
[3] *ELETTRA – Sincrotrone Trieste, S.S. 14 in Area Science Park, I-34149 Basovizza, Trieste, Italy*

**emmanuel.nolot@cea.fr*

Abstract

Advanced chalcogenide materials are key for state-of-the art memories, energy harvesting materials and photonics. The properties of thin chalcogenide layers are highly driven by their chemical composition, chemical depth-profiles and surface/interface effects. The combination of Grazing-Incidence X-ray Fluorescence (GIXRF) and X-ray Reflectometry (XRR) techniques allows for non-destructive access to such information, in the lab or at dedicated beamlines. However, the accuracy of the GIXRF-deduced composition slightly degrades with depth, as the enhancement of the XRF signal by the X-ray Standing Wave (XSW) field is usually limited to the first nanometers at the surface of the probed sample. In this paper, we suggest the use of (Mo/Si)*N Bragg mirrors, rather than bare silicon substrates for thin chalcogenide deposition, to improve the sensitivity of GIXRF/XRR analysis to small process-driven modifications. The aim of such multilayered substrates is to maintain high values of X-ray reflected intensity even at angles significantly higher than the critical angle, therefore generating an XSW-induced enhancement of the XRF signal not only at the surface but also in the depth of the layer of interest. The simulation of GIXRF-XRR data, collected at SOLEIL Metrology beamline and in the lab on Rigaku SmartLab diffractometer, on arsenic-free Ovonic Threshold Switch materials (Ge, Se, Sb) for advanced Phase Change memory (PCRAM) applications illustrates the interest of this approach, which is fully-compatible with numbers of PCRAM materials elaborated with low-temperature physical vapor deposition process.

Key-Words: Grazing-incidence X-ray fluorescence; X-ray fluorescence; chalcogenides; combined analysis; phase-change memory

1. Introduction

The combination of grazing-incidence X-ray fluorescence (GIXRF) with X-ray reflectometry (XRR) is particularly adequate to probe thin layered materials at industrial level (i.e. the semiconductor industry) [1-5]. GIXRF is a highly sensitive elementary technique capable to probe chemical depth profiles in films with thickness ranging from few nm to ~ 200 nm. GIXRF was formalized by De Boer in the early 90's and recently gained widespread interest to semiconductor industry due to device miniaturization [6-10]. On the other hand, XRR technique is a well-established technique widely available in labs and fabs, which provides accurate values of mass density, thickness and roughness of smooth layered films [11] in almost the same thickness range as GIXRF. The key advantage of combining XRR with GIXRF is in the drastic reduction of the cross-correlated parameters' dependencies, e.g. between thickness and mass density in GIXRF-only analysis [12]. GIXRF/XRR combines electronic density (XRR) and atomic density (GIXRF) profiles, resulting in improved ability to determine accurate quantitative chemical depth-dependent information in thin layered materials.

In GIXRF experiment conducted on flat surfaces, which is often the case when thin layered materials are grown on silicon substrates, the monochromatic low-divergence primary beam interferes with the reflected beam, thereby generating an X-ray standing wave (XSW) field at the surface of the sample. The intensity of the XSW field strongly varies with the depth and the incident angle, resulting in an XSW-induced enhancement of the emitted fluorescence intensity. However, the sensitivity of GIXRF slightly degrades with depth, as the enhancement of the XRF signal by the X-ray Standing Wave (XSW) field is usually limited to the first nanometers at the surface of the probed sample. As illustrated by Eq(1) in the case of a thick substrate [13], the enhancement factor A_{XSW} of the fluorescence intensity is driven by the reflectivity

$$A_{XSW}(\theta, z) = 1 + R(\theta) + 2 * \sqrt{R(\theta)} \cos\left(\frac{2\pi z \sin\theta}{\lambda} - \varphi(\theta)\right) \quad \text{Eq(1)}$$

Where θ is the glancing angle, z the depth, $R(\theta)$ the reflectivity, λ the wavelength of the monochromatic X-ray beam and φ the phase difference between the incident and the reflected waves. Therefore, the sensitivity of GIXRF at high (> 5-10 nm) depth may be improved by a significant increase of the reflectivity at angles larger than the

critical angle, for instance by virtue of multi-layered Bragg mirrors. Note that the careful modeling of the XSW field has been used to support improved GIXRF characterization of multilayers [14] or even of periodic nanostructures [15-17].

Advanced chalcogenide materials, based on tellurium, selenium or sulfur, are key for state-of-the art memories such as phase change random access memory (PCRAM), energy harvesting materials and photonics. PCRAM are already produced in advanced fabs (e.g in Resistive Memory Crossbar products such as Intel 3D XPoint^{TM}), and extensive research is being conducted to optimize their properties, for instance for automotive applications. PCRAM include two main complex thin materials: a chalcogenide phase change material (PCM) and a selector material, which is required to limit sneak paths issues such as reading fail and cell-to-cell disturbance in Resistive Memory Crossbar architectures. Selenium-based materials are investigated as arsenic-free solution for the selector material; for instance, Ge-rich GeSe chalcogenides feature promising characteristics such as a high resistance of the Off state, and a reasonable threshold voltage when doped with antimony [18]. The properties of thin chalcolgenide layers are highly driven by their chemical composition, chemical depth-profiles and surface/interface effects [19]. Lencer et al [20] built a map of chalcogenide materials that enables to identify suitable phase change materials on the basis only of the material stoichiometry. Similarly, Kau et al demonstrated that the selector scales with PCM, physically, chemically, and electrically [21].

Thin amorphous chalcogenide films can be deposited by magnetron sputtering technique with limited thermal budget (deposition temperature ~ 60°C) that will not modify the properties of (Mo/Si)*N Bragg mirrors used as alternative substrates. Thin chalcogenide stacks are consequently particularly suitable to illustrate the effectiveness of alternative substrates for GIXRF analysis. In this paper, we suggest the use of (Mo/Si)*N Bragg mirrors rather than bare silicon substrates for thin chalcogenide deposition in order to improve the sensitivity of GIXRF/XRR analysis to small process-driven modifications.

2. Experimental

2.1. Sample preparation

We deposited germanium-selenium films on 200 mm silicon (001) wafers using magnetron sputtering technique in an Evatec Clusterline 200 multi-target chamber. We acquired high quality Bragg mirrors, grown on silicon substrate and consisting of 40 pairs of {Si (5 nm)/ Mo (2 nm)}, from Applied X-ray optics AXO Dresden GmbH Company. We cut these multilayer substrates and attached one part to the 200 mm silicon wafer for each process condition, so as to generate exact duplicated samples on silicon and Bragg mirror substrates.

We deposited different materials and stacks: individual GeSe films (using a GeS_2 target), Sb-doped GeSe films (by co-sputtering of Sb and $GeSe_2$ targets), and bilayer samples consisting of undoped and Sb-doped GeSe films. The thickness of each individual layer was set to 10 nm. Finally, we capped the thin chalcogenide materials with a 5-nm thick amorphous carbon layer deposited *in situ* (no air break) in order to limit ageing-induced concern during the characterization process [22]. We referenced the samples as indicated hereafter:

- Sample a1 : C (5 nm) / GeSe (10 nm) / GeSeSb (10 nm) / Si substrate
- Sample a2: C (5 nm) / GeSeSb (10 nm) / GeSe (10 nm) / Si substrate
- Sample b1 : C (5 nm) / GeSe (10 nm) / GeSeSb (10 nm) / Bragg mirror
- Sample b2: C (5 nm) / GeSeSb (10 nm) / GeSe (10 nm) / Bragg mirror

2.2. Characterization

We first conducted XRR and wavelength dispersive XRF (WDXRF) experiments in the cleanroom in order to determine the thickness, and the mass density of the layers, and the global composition of the deposited materials. In addition, inline XRR-WDXRF with dedicated mapping permits to control the quality of the deposition and its uniformity at the wafer scale. We performed in-line XRR analysis on a Bruker D8 Fabline tool based on theta-theta geometry and using Cu-Kα (8.048 keV) with limited divergence (1.2 mrad) as primary radiation. In-line WDXRF experiments were carried out in the primary-vacuum chamber of Rigaku AZX400 instrument. The samples were irradiated with the polychromatic X-ray radiation emitted by a Rhodium tube operated at 40 kV and 75 mA. We used a Lithium fluoride crystal LiF 200 (resp. a synthetic crystal with 2d = 3.04 nm) mounted on a high-resolution goniometer to select the wavelengths related to Sb-Lα and Se-Kα (resp. Ge-Lα) lines. The X-ray fluorescence intensities were recorded with a gas flow type proportional counter (for Ge-Lα and Sb-Lα) and with a scintillator (for Se-Kα).

We performed GIXRF experiment, first in the lab to probe Sb-Lα fluorescence line, then at the Metrology beamline of SOLEIL synchrotron, in order to access Se-Kα and Ge-Kα fluorescence lines. In the lab, we used Rigaku SmartLab five-axis high-resolution diffractometer, operated at atmospheric pressure to probe the Sb-Lα fluorescence line at 3.605 keV. We conditioned the X-ray beam produced by the 9 kW rotating copper anode in order to deliver a 30 µm-width monochromatic beam (Cu-$K\alpha_1$, 8.048 keV) with 0.2 mrad divergence on the sample. We acquired the X-ray fluorescence signal with a Hitachi Vortex 90EX silicon drift detector (SDD) mounted on a customized set-up provided by Rigaku. The SDD detector was placed at 90° from the sample surface, 10 mm above the sample. At the Metrology beamline, we acquired GIXRF data on the hard X-ray energy

branch (available range: 3 to 35 keV) of the Metrology beamline at the SOLEIL synchrotron, using high-vacuum CASTOR analysis chamber [23] and equipped with a silicon drift detector (SDD) mounted at 90° with respect to the sample surface. We chose 13.5 keV as excitation energy, i.e slightly above Se-K and Ge-K edges in order to optimize for the detection of Se-Kα (11.222 keV) and Ge-Kα (9.886 keV).

Complementary time-of-flight secondary ion mass spectrometry (ToF-SIMS) experiments were carried out using an ION TOF GmbH TOF SIMS 5 equipped with a Bi liquid metal ion gun and a Cs sputter source. Depth profiles were performed in the non-interlaced mode (separate cycles for analysis, sputtering, and charge compensation) with Cs sputtering incident at 45°. The analysis was performed using the bismuth analysis gun incident at 45° with an impact energy of 25 keV, and Bi^{3+} primary ions were used to enhance the MCsn+ secondary ion yield in the positive mode.

2.3. Analysis software and sample design

We used Rigaku proprietary software based on fundamental parameters to analyze the inline WDXRF data. XRR-GIXRF analysis was performed with Medepy software (using PyMCA [24] to first extract the fluorescence integrated intensities), developed at Cea-Leti, and which allows the combined analysis of multiple datasets collected on different instruments that may feature different instrumental functions and distinct primary energy [25]. In addition, Medepy permits to evaluate the XSW-enhancement of the fluorescence signal. We used this capability to define the thicknesses of the molybdenum and the silicon layers along with the number of pairs in the Bragg mirror, in order to tune the positions of the maxima of the XSW field, and therefore the sensitivity of GIXRF to different depth positions, in the capping layer, then in undoped and Sb-doped layers, for Cu-Kα primary energy (Fig.1).

3. Results and discussion

3.1 Inline XRR and WDXRF characterization

Prior to any deposition, we measured the multilayer substrates provided by AXO with Bruker D8 Fabline inline XRR tool. The XRR data (Fig.2) highlight the expected presence of well-defined Bragg peaks and were reasonably modeled using 40 pairs of molybdenum (2.0 nm; 10.2 g/cm^3) - silicon (5.0 nm; 2.33 g/cm^3) bilayer. We used a 1.5 nm-thick SiO_2 layer to account for the oxidation of the top (silicon) layer of the multilayer substrates. Silicon and molybdenum layers feature XRR-deduced roughness of 0.3 and 0.4 nm respectively, which slightly lowers the reflectivity at the position of the two first Bragg peaks (reflectivity equals 0.84 and 0.33 respectively) when compared to expectation. As the intensity of higher order Bragg peaks is less than 0.1, we expect significant XSW-induced enhancement of the XRF signal close to the position of the two first Bragg peak only.

We used inline WDXRF and fundamental parameters approach [26] to quantify the deposited mass of germanium, selenium and antimony on samples a1, a2, b1 and b2. In order to determine the spectrometer sensitivity values required for WDXRF-based quantification, we used pure germanium and antimony targets, along with a selenium-rich $Ge_{0.3}Se_{0.7}$ PVD target. The quantified values are listed in the Table 1, which clearly shows that the samples deposited on silicon and multilayer substrates are almost perfect duplicates.). To build rigorous uncertainty budget related to such inline WDXRF quantitative analysis appears rather difficult, since we do not have access to some proprietary information such as the database used of fundamental parameters. Nevertheless, we can reasonably expect a global accuracy in the 1 at% range (absolute), based on recent studies conducted on thin inorganic films using the same WDXRF tool and similar quantification methodology [27, 28]

Sample	Ge	Sb	Te	Ge	Sb	Te
	Deposited mass (µg/cm²)				*%at*	
a1	2.11	1.20	7.15	30.6	10.4	59.0
a2	2.13	1.11	7.24	30.8	9.6	59.6
b1	2.11	1.17	7.36	30.0	10.0	60.0
b2	2.08	1.17	7.34	29.9	10.0	60.1

Table 1: Deposited mass of germanium, antimony and tellurium deduced from WDXRF analysis, and related composition of the thin chalcogenide material

3.2 GIXRF characterization and TOF-SIMS analysis

Inline WDXRF and XRR analysis do not provide accurate information on the depth-dependent characteristics of the thin layered samples: WDXRF does not feature in-depth sensitivity, whereas the density of undoped and Sb-doped GeSe thin materials are too close to allow unambiguous depth-dependent information based only on XRR.

We ran qualitative TOF-SIMS on samples a1 and a2 in order to evidence the difference between undoped and Sb-doped GeSe layers in the two distinct stacks (Fig. 3) and to confirm the lack of diffusion of germanium, selenium and antimony in the carbon layer. The different materials come with significantly different relative sensitivity factors (RSF: Sb > Ge > Se, with possible differences between RSF in GeSe and GeSeSb layers). Therefore, we can only suggest, based on Fig.3, that the addition of antimony in the germanium selenide might decrease the selenium content in the material. However, the comparison with WDXRF quantification of elementary samples (GeSe and GeSeSb) shows that the addition of up to 18 at% of antimony leads to negligible modification in the Se/Ge ratio.

We conducted GIXRF experiments in the Lab, then at the Metrology beamline at SOLEIL. In both cases, we used elementary samples to determine the instrumental function of the GIXRF tool, following the methodology explained in [1]. The experiments were performed at two monochromatic excitation energies (8.048 keV and 13.5 keV) and the related illustrations, such as angle-dependent XRF intensity graphs, are plotted against the scattering vector ($q = 4\pi\sin\theta/\lambda$) for sake of clarity. Figures 4 and 5 show the angle-dependent XRF intensity of Si-Kα and Sb-Lα as measured on the SmartLab tool for **a** and **b** samples. Angle-dependent Si-Kα has a bulk-like behavior for **a** samples whereas the presence of silicon in the multilayer substrates results in added features at Bragg peak positions for **b** samples. The order of the layers in the stacks is clearly highlighted by the angle-dependent Sb-Lα graphs, for both **a** and **b** samples. Higher intensity of Sb-Lα below the critical angle is a clear and unambiguous indication the Sb-doped GeSe materials are the upper layers in a2 and b2 samples. In addition, the intensity of Sb-Lα far above the critical angle ($q > 3.q_c$) is almost identical, which is consistent with almost identical deposited mass of antimony deduced from WDXRF analysis (Table 1). Lastly, we notice that the angle-dependent Sb-Lα graphs show additional features around the first Bragg peak that should reinforce the sensitivity of GIXRF. As expected from the XRR analysis of the multilayer substrates, the Bragg peaks of higher orders do not contribute to this potential increase of sensitivity.

We faced some unexpected difficulties when running the GIXRF experiment at the Metrology beamline, and we could not properly measure samples a2 and b1, which limits our ability to quantify the added sensivity of multilayer substrate approach. We used Medepy software to model the data of sample b2, combining XRR acquired inline, Sb-Lα GIXRF data collected in the Lab at 8.048 keV and Se-Kα and Ge-Kα GIXRF data acquired at the beamline at 13.5 keV. We used the Névot-Croce model to describe the top and interfacial roughness, and xraylib [29] as database for optical constants. The GIXRF and XRR instrumental functions were evaluated from the data collected on elementary sample. Then, we performed the analysis of b2 sample (Fig. 6) with fixed instrumental functions, by virtue of careful refinement of thickness, density, roughness and composition of the thin-layered materials based on simultaneous analysis of GIXRF and XRR data.

4. Conclusions

GIXRF/XRR combined analysis can reveal the depth-dependent characteristics of thin-layered materials for advanced memory in a non-destructive manner, which is particularly suitable for inline metrology. As suggested by the good results obtained with SmartLab lab tool, a lab or inline tool that would combine two primary energy (e.g Cu-Kα and Mo-Kα), low divergence and small spot capability, would certainly fit the requirement for inline non-destructive depth-dependent compositional analysis at the wafer level. The introduction of carefully designed multilayer substrates, with optimized reflected intensity of the two first Bragg peaks, should increase the sensitivity of GIXRF to small process-induced variability. The characteristics of (Mo/Si)-based multilayer substrates do not degrade during the low-temperature physical vapor deposition process of numbers of PCRAM materials, whereas multilayers with optimized composition can offer stability up to 500°C [30], thereby extending the range of acceptable material deposition process. In addition, as only small parts of such substrates could be attached to silicon wafer during the deposition process, the related added cost would be negligible.

Acknowledgments

The financial support of the EMPIR program is gratefully acknowledged. It is jointly funded by the European Metrology Programme for Innovation and Research (EMPIR) and participating countries within the European Association of National Metrology Institutes (EURAMET) and the European Union.

We acknowledge SOLEIL for provision of synchrotron radiation facilities and we would like to thank Pascal Mercere and Paulo Da Silva for assistance in using beamline “Metrology."

5. References

[1] H. Rotella, B. Caby, Y. Ménesguen, Y. Mazel, A. Valla, D. Ingerle, B. Detlefs, M.-C. Lépy, A. Novikova, G. Rodriguez, C. Streli, E. Nolot, *Elemental depth profiling in transparent conducting oxide thin film by X-ray reflectivity and grazing incidence X-ray fluorescence combined analysis*, Spectrochimica Acta Part B 135 (2017): 22-28, http://dx.doi.org/10.1016/j.sab.2017.06.011

[2] B. Caby, F. Brigidi, D. Ingerle, E. Nolot, G. Pepponi, C. Streli, L. Lutterotti, A. André, G. Rodriguez, P. Gergaud, M. Morales, D. Chateigner, *Study of annealing-induced interdiffusion in In_2O_3/Ag/In_2O_3 structures by a combined X-ray reflectivity and grazing incidence X-ray fluorescence analysis*, Spectrochimica Acta, Part B 113 (2015) 132–137, http://dx.doi.org/10.1016/j.sab.2015.09.008.

[3] P. Hönicke, B. Detlefs, E. Nolot, Y. Kayser, U. Mühle, B. Pollakowski, B. Beckhoff, *Reference-free grazing incidence x-ray fluorescence and reflectometry as a methodology for independent validation of x-ray reflectometry on ultrathin layer stacks and a depth-dependent characterization*, J. Vac. Sci. Technol., A (2019) 37, 041502, https://doi.org/10.1116/1.5094891

[4] E. Nolot, B. Caby, R. Gassilloud, M. Veillerot, D. Eichert, *X-ray reflectometry and grazing-incidence X-ray fluorescence characterization of innovative electrodes for tantalum-based resistive random access memories*, Spectrochimica Acta, Part B, 149 (2018) 71-75, https://doi.org/10.1016/j.sab.2018.07.017

[5] W. Pessoa, A. Roule, E. Nolot, Y. Mazel, M. Bernard, M.-C. Lépy, Y. Ménesguen, A. Novikova, P. Gergaud, F. Brigidi, D. Eichert, *Grazing incident X-ray fluorescence combined with X-ray reflectometry metrology protocol of telluride-based films using in-lab and synchrotron instruments*, Spectrochimica Acta, Part B, 149 (2018) 143-149, https://doi.org/10.1016/j.sab.2018.07.003

[6] A.J.G. Leenaers, J.J.A.M. Vrakking, D.K.G. De Boer, *Glancing incidence X-ray analysis: more than just reflectivity!*, Spectrochimica Acta B 52 (7) (1997) 805–812, https://doi.org/10.1016/S0584-8547(96)01651-5.

[7] D.K.G. De Boer, A.J.G. Leenaers, W.W. Van Den Hoogenhof, *Glancing-incidence x-ray analysis of thin-layered materials: A review*, X-Ray Spectrom. 24 (3) (1995) 91–102, https://doi.org/10.1002/xrs.1300240304

[8] D.K.G. de Boer, *Glancing-incidence X-ray fluorescence of layered materials*, Phys. Rev. B 44 (1991) 498–511, https://doi.org/10.1103/PhysRevB.44.498

[9] J. Lubeck, B. Beckhoff, R. Fliegauf, I. Holfelder, P. Hönicke, M. Müller, B. Pollakowski, F. Reinhardt, J. Weser, *A novel instrument for quantitative nanoanalytics involving complementary X-ray methodologies*, Rev. Sci. Instrum. 84 (2013) 045106, https://doi.org/10.1063/1.4798299

[10] V. Szwedowski-Rammert, J. Baumann, C. Schlesiger, U. Waldschläger, A. Gross, B. Kanngießer, and I. Mantouvalou, *Laboratory based GIXRF and GEXRF spectrometers for multilayer structure investigations*, J. Anal. At. Spectrom., 2019, 34, 922, https://doi.org/10.1039/c8ja00427g

[11] L. G. Parratt, *Surface Studies of Solids by Total Reflection of X-Rays*, Phys. Rev 95 (1954) 359–369., https://doi.org/10.1103/PhysRev.95.359

[12] D. Ingerle, G. Pepponi, F. Meirer, P. Wobrauschek, C. Streli, *A multiplatform code for the analysis of energy-dispersive X-ray fluorescence spectra*, Spectrochimica Acta B 118 (2016) 20–28, https://doi.org/10.1016/j.sab.2006.12.002.

[13] R. Klockenkamper, *Total-Reflection X-Ray Fluorescence Analysis and Related Methods*, Eds Wiley and sons (2015)

[14] Y. Tu, Y. Yuan, K. Le Guen, J-M André, J. Zhu, Z. Wang, F.Bridou, A. Gigliae and P. Jonnard, *X-ray fluorescence induced by standing waves in the grazing-incidence and grazing-exit modes: study of the Mg–Co–Zr system*, J. Synchrotron Rad. (2015). 22, 1419-1425, https://doi.org/10.1107/S1600577515016239

[15] V. Soltwisch, P. Hönicke, Y. Kayser, J. Eilbracht, J. Probst, F. Scholze and B.Beckhoff, *Element sensitive reconstruction of nanostructured surfaces with finite elements and grazing incidence soft X-ray fluorescence*, Nanoscale, 2018, 10, 6177–6185, https://doi.org/10.1039/c8nr00328a

[16] K. V. Nikolaev, V. Soltwisch, P. Hönicke, F. Scholze, J. de la Rie, S. N. Yakunin, I. A. Makhotkin, R. W. E. van de Kruijs and F. Bijkerk, *A semi-analytical approach for the characterization of ordered 3D nanostructures*

using grazing-incidence X-ray fluorescence, J. Synchrotron Rad. (2020). 27, 386-395, https://doi.org/10.1107/S1600577519016345
[17] S.H. Nowak, D. Banaś, W. Błchucki, W. Cao, J.-Cl. Dousse, P. Hönicke, J. Hoszowska, Ł. Jabłoński, Y. Kayser, A. Kubala-Kukuś, M. Pajek, F. Reinhardt, A.V. Savu, J. Szlachetko, *Grazing angle X-ray fluorescence from periodic structures on silicon and silica surfaces*, Spectrochimica Acta Part B: Atomic Spectroscopy 98 (2014), 65-75, https://doi.org/10.1016/j.sab.2014.03.015
[18] A. Verdy A., M. Bernard, J. Garrione, G. Bourgeois, M.C. Cyrille, E. Nolot, N. Castellani, P. Noe, C. Socquet-Clerc, T. Magis, G. Sassine, G. Molas, G. Navarro, E. Nowak, *Optimized Reading Window for Crossbar Arrays Thanks to Ge-Se-Sb-N-based OTS Selectors*, Technical Digest - International Electron Devices Meeting, IEEE International Electron Devices Meeting (IEDM), pp. 37.4.1-37.4.4, December 2018, https://doi.org/10.1109/IEDM.2018.8614686
[19] H. Y. Cheng, T. H. Hsu, S. Raoux, J.Y. Wu, P. Y. Du, M. Breitwisch, Y. Zhu, E. K. Lai, E. Joseph, S. Mittal, R. Cheek, A. Schrott, S. C. Lai, H. L. Lung, and C. Lam , *A high performance phase change memory with fast switching speed and high temperature retention by engineering the GexSbyTez phase change material*, 2011 IEEE International Electron Devices Meeting (IEDM), pp. 3.4.1–3.4.4, December 2011
[20] D. Lencer, M. Salinga, B. Grabowski, T. Hickel, J. Neugebauer and M. Wuttig, *A map for phase-change materials*, Nature materials Vol 7, pp 972-977, December 2008
[21] D.C. Kau, S. Tang, I.V. Karpov, R.Dodge, B. Klehn, J.A. Kalb, J. Strand, A. Diaz, N. Leung, J. Wu, S. Lee, T. Langtry, K. Chang, C. Papagianni, J. Lee, J. Hirst, S. Erra, E. Flores, N. Righos, H. Castro and G. Spadini, *A stackable cross point phase change memory*, 2009 IEEE International Electron Devices Meeting (IEDM), pp 27.1;1-27.1.4, December 2009
[22] A. Verdy, G. Navarro, M. Bernard, S. Chevalliez, N. Castellani, E. Nolot, J. Garrione, P. Noé, G. Bourgeois, V. Sousa, M.C. Cyrille and E. Nowak, *Carbon electrode for Ge-Se-Sb based OTS selector for ultra low leakage current and outstanding endurance*, IEEE International Reliability Physics Symposium Proceedings, March 2018, pp. 6D.41-6D.46, https://doi.org/10.1109/IRPS.2018.8353635
[23] Y. Ménesguen B. Boyer H. Rotella J. Lubeck J. Weser B. Beckhoff D. Grötzsch B. Kanngießer , A. Novikova E. Nolot M.-C. Lépy, *CASTOR, a new instrument for combined XRR-GIXRF analysis at SOLEIL*, X-Ray Spectrom. 2017, 46, 303–308, https://doi.org/10.1002/xrs.2742
[24] V. Solé, E. Papillon, M. Cotte, P. Walter, J. Susini, *A multiplatform code for the analysis of energy-dispersive X-ray fluorescence spectra*, Spectrochim. Acta B At. Spectrosc. 62 (2007) 63–68, https://dx.doi.org/10.1016/j.sab.2006.12.002
[25] B. Caby, F. Brigidi, D. Ingerle, B. Detlefs, G. Picot, L. Lutterotti, E. Nolot, G. Pepponi, C. Streli, M. Morales, D. Chateigner, *Comparison of four data analysis software for combined X-ray reflectivity and grazing incidence X-ray fluorescence measurements*, TXRF conference, 2015
[26] M. Mantler, J.P Willis, G.R Lachance, B.A.R Vrebos, K.E Mauser, N. Kawahara, R.M Rousseau, P.N Brouwer, B. Beckhoff, B. Kanngiesser, N. Langhoff, R. Wedell, H. Wolff, H., *Handbook of Practical X-Ray Fluorescence Analysis*, Eds.; Springer: Berlin, Germany, 2006; pp. 309–410.
[27] E.Nolot, S. Cadot, F.Martin, P.Hönicke, C.Zech, B.Beckhoff, *In-line characterization of ultrathin transition metal dichalcogenides using X-ray fluorescence and X-ray photoelectron spectroscopy*, Spectrochimica Acta Part B 166 (2020) 105788, https://doi.org/10.1016/j.sab.2020.105788
[28] C. Jeynes, E. Nolot, C. Costa, C. Sabbione, W. Pessoa, F. Pierre, A. Roule, G. Navarro, and M. Mantler, *Quantifying nitrogen in GeSbTe:N alloys*, J. Anal. At. Spectrom., 2020,35, 701-712, https://doi.org/10.1039/c9ja00382g
[29] T. Schoonjans, A. Brunetti, B. Golosio, M. Sanchez del Rio, V. A. Solé, C. Ferrero and L. Vincze, *The xraylib library for X-ray–matter interactions. Recent developments*, Spectrochimica Acta Part B 66 (2011) 776–784, https://doi.org/10.1016/j.sab.2011.09.011
[30] S.Yulin, N. Benoit, T. Feigl and N. Kaiser, *Interface-engineered EUV multilayer mirrors*, Microelectronic Engineering 83 (2006) 692–694, https://doi.org/10.1016/j.mee.2006.01.126

6. Figures and captions

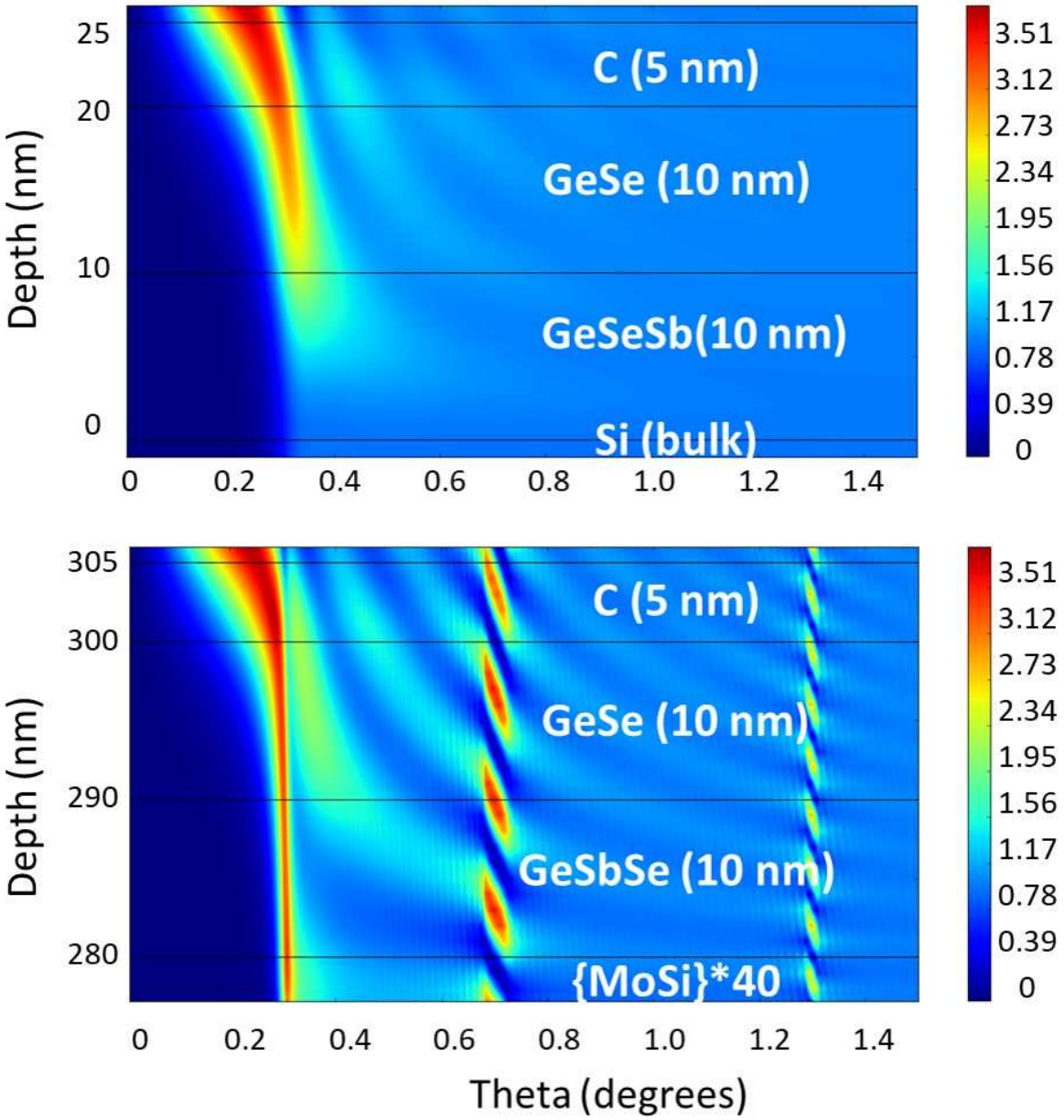

Figure 1. In-depth distribution of the X-ray standing wave field in targeted stacks of samples a1 deposited on silicon and b1 deposited on MoSi Bragg mirror, as simulated with Medepy software at Cu-Kα primary energy.

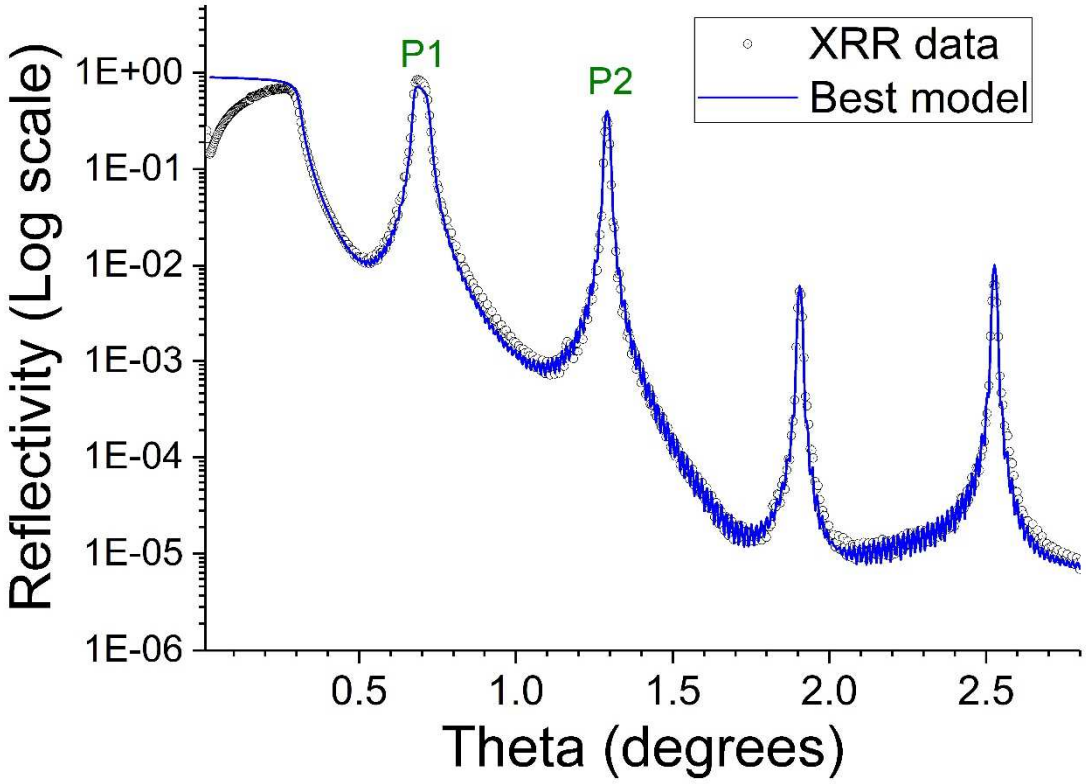

Figure 2. XRR data of (Mo/Si)*40 substrate (provided by AXO) collected on inline Bruker D8 Fabline tool operated at 8.048 keV, along with best-model calculation. P1 and P2 indicate the positions of the two first Bragg peaks.

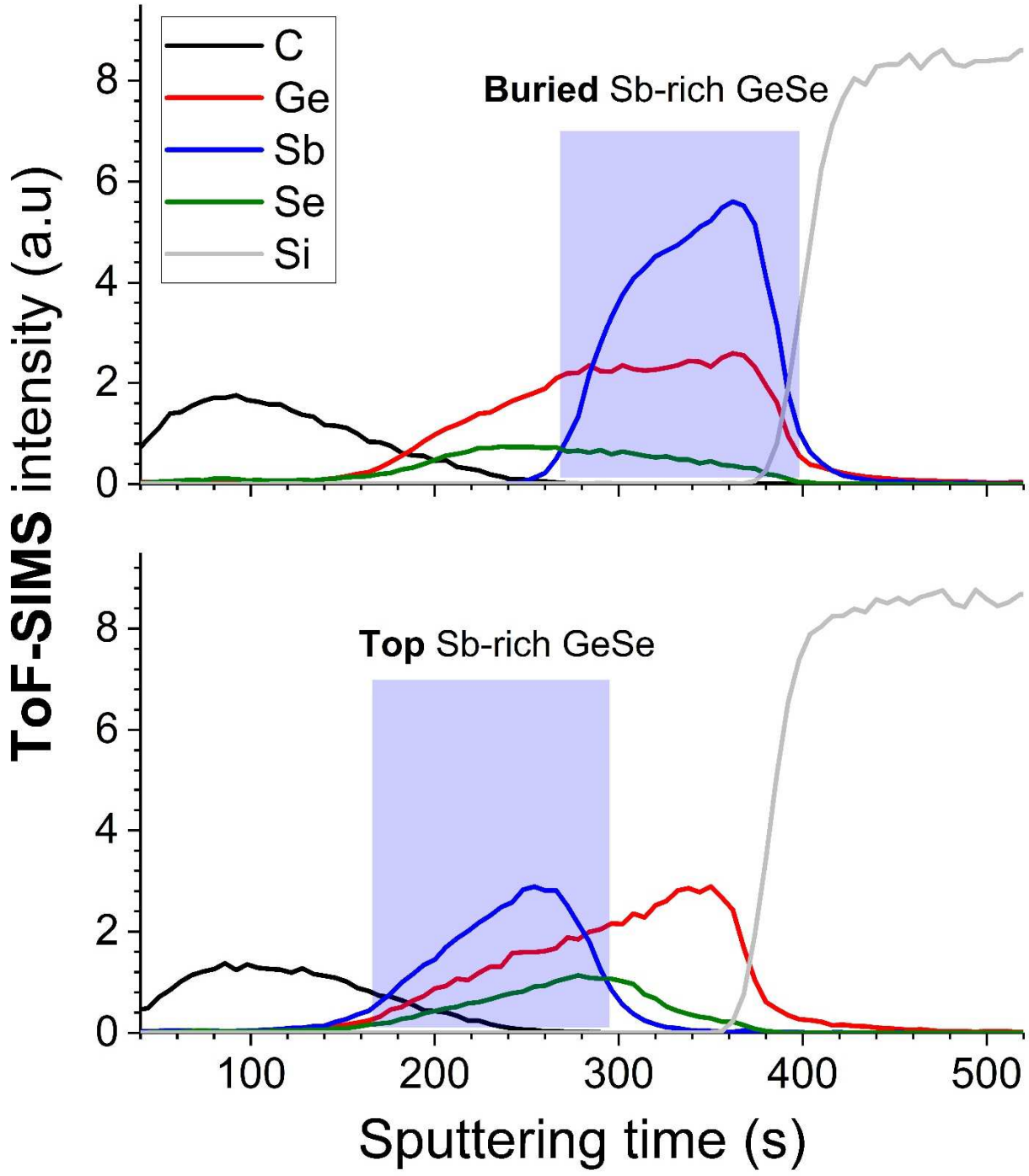

Figure 3. Chemical depth-profiles in samples a1 (buried Sb-rich GeSe) and a2 (top Sb-rich GeSe) as measured by TOF-SIMS, using C+, $GeCs_2$+, SeCs+, $SbCs_2$+, and $SiCs_2$+ ions to monitor C, Ge, Se, Sb and Si respectively.

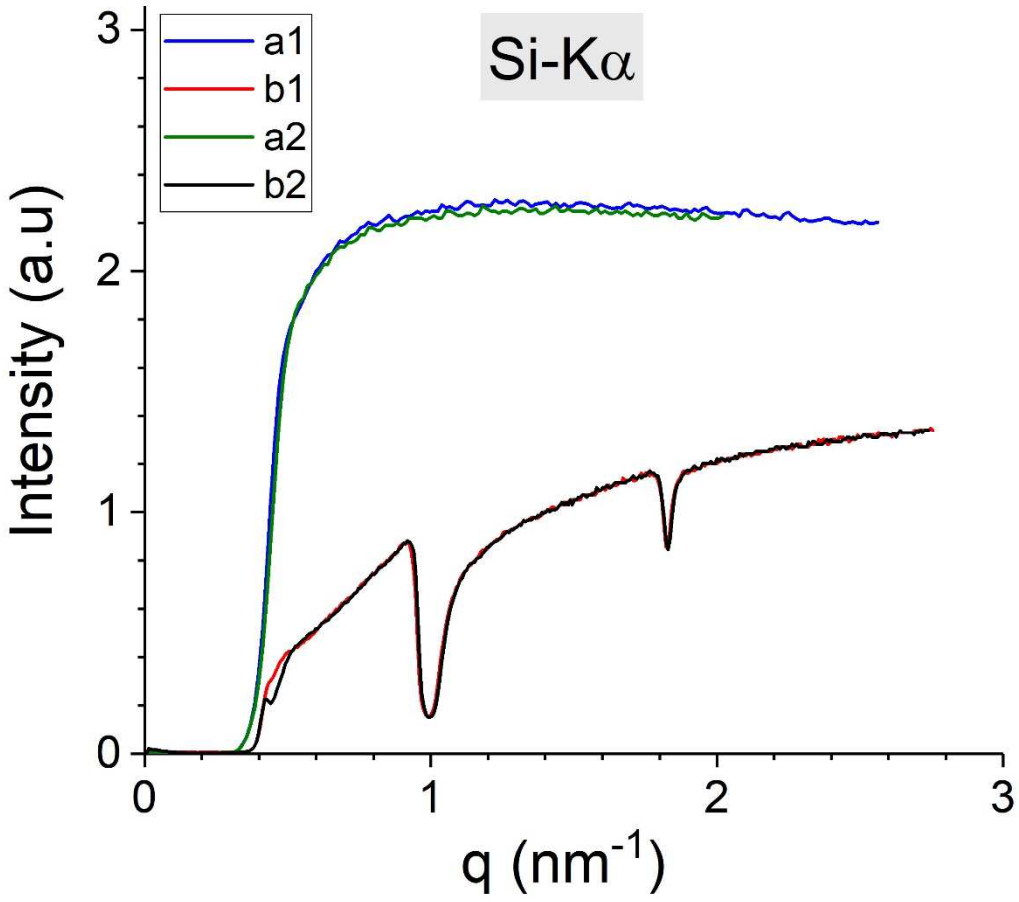

Figure 4. Comparison of the angle-dependent fluorescence intensity of Si-Kα line measured with SmartLab lab tool at Cu-Kα primary energy

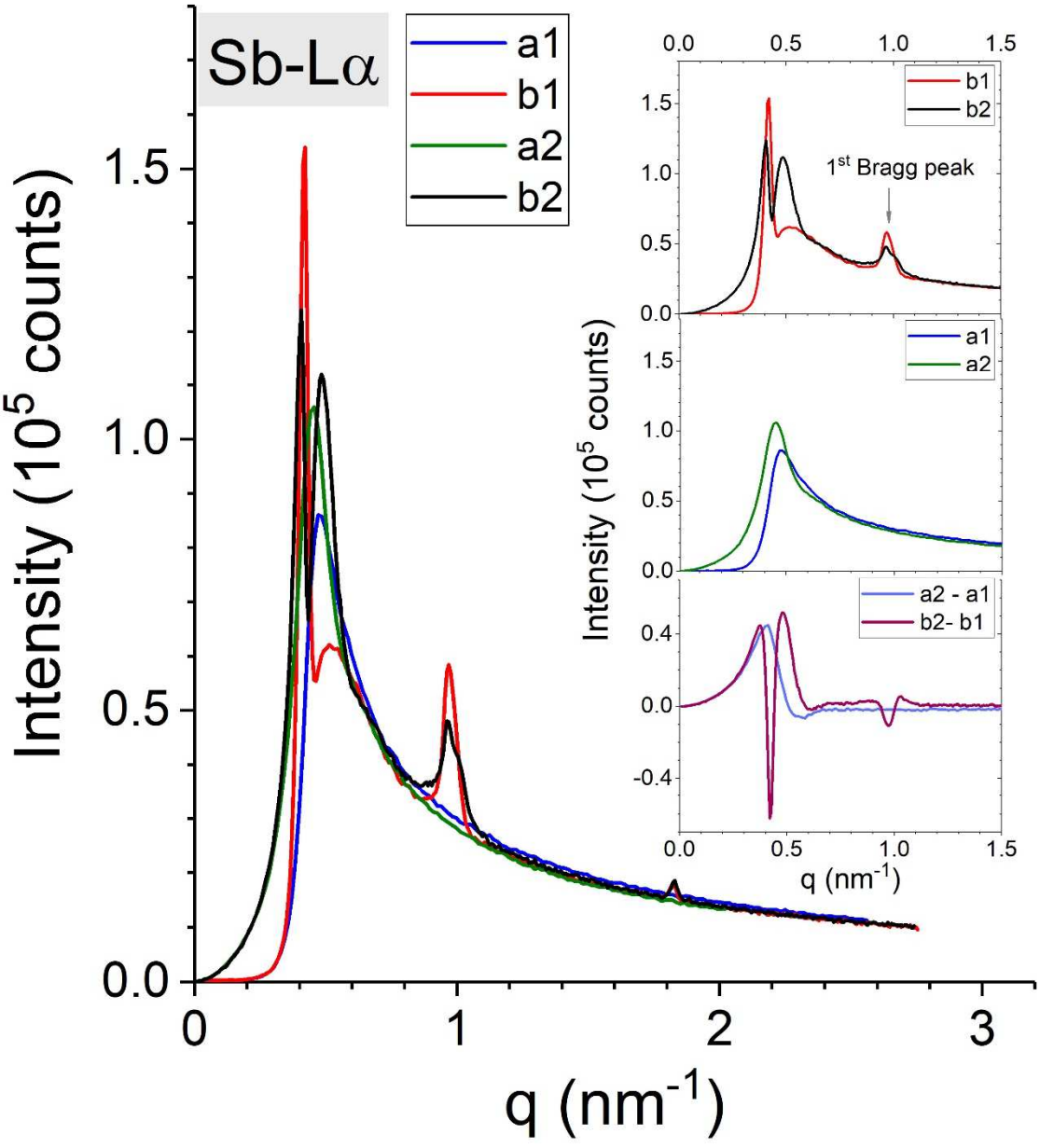

Figure 5. Comparison of the angle-dependent fluorescence intensity of Sb-Lα line measured with SmartLab lab tool at Cu-Kα primary energy

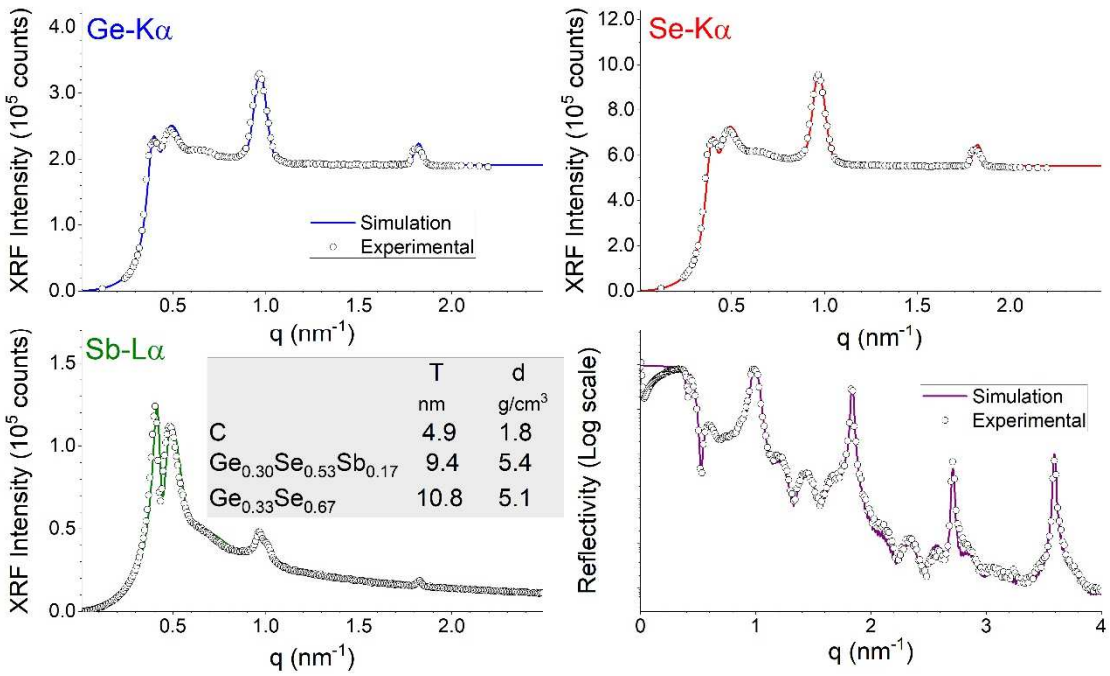

Figure 6. Experimental GIXRF-XRR data and best model calculation for sample b2. We collected the XRR data with inline Bruker D8 Fabline tool at 8.048 keV, the Sb-Lα XRF data in the lab on Rigaku SmartLab tool operated at 8.048 keV, and Se-Kα and Ge-Kα XRF data at the Soleil Metrology beamline using 13.5 keV excitation energy

Graphical abstract